Available online at www.sciencedirect.com
SCIENCE DIRECT®
Coordination Chemistry Reviews 248 (2004) 1231–1246
COORDINATION CHEMISTRY REVIEWS
www.elsevier.com/locate/ccr

Review

Ultrafast electron injection from metal polypyridyl complexes to metal-oxide nanocrystalline thin films

Neil A. Anderson, Tianquan Lian*

Department of Chemistry, Emory University, Atlanta, GA 30322, USA

Received 14 November 2003; accepted 15 March 2004
Available online 10 August 2004

Contents

Abstract

Interfacial electron transfer (ET) between molecular adsorbates and semiconductor nanoparticles has been a subject of intense recent interest. In this paper, we review our recent work in understanding ultrafast photoinduced electron injection from ruthenium and rhenium polypyridyl complexes to metal oxide nanoparticles. Electron injection rates were measured using femtosecond IR spectroscopy, which provided a direct probe of adsorbate vibrational spectra and IR absorption of injected electrons in semiconductor. The consequence of competition between ultrafast electron injection and intramolecular relaxation in these transition metal complexes was carefully examined. A two-state injection model was proposed to account for biphasic kinetics, allowing a comparison of injection rate in different systems. The components of the chromophore(donor)–bridge–nanoparticle (acceptor) complexes were systematically varied to examine their effect on ET rate. The observed trends were discussed by considering the change in the strength of electronic coupling and density of accepting states in semiconductor and compared with Marcus theory of interfacial electron transfer.

Keywords: Electron transfer (ET); Electron injection; Thin film

* Corresponding author. Tel.: +1 4047276649; fax: +1 4047276586.
E-mail address: tlian@emory.edu (T. Lian).

0010-8545/$ – see front matter © 2004 Elsevier B.V. All rights reserved.
doi:10.1016/j.ccr.2004.03.029

1. Introduction

Interfacial electron transfer (ET) between molecular adsorbates and semiconductor nanoparticles has been a subject of intense recent interest [1–6], because of their applications in solar energy conversion [7–9], photocatalysis [5,10], and nano-scale and molecular electronics [11–16]. An interesting application enabled by the large surface area of semiconductor nanoparticles is novel hybrid solar cells based on composites of molecular and nanostructured semiconductor components, such as dye-sensitized nanocrystalline thin film [7,8] and quantum dot/conjugated polymer [9,17,18] and related composites [19,20]. These cells may provide cost-effective alternatives to traditional semiconductor-based cells. In these devices, the interface between semiconductor and the molecule forms a photoactive junction and the incident photon-to-current conversion efficiency (IPCE) depends critically on its area and charge separation dynamics. Presently, the most efficient cells of this type, dye-sensitized solar cells based on $Ru(dcbpy)_2(NCS)_2$ [dcbpy = (4,4′-dicarboxy-2,2′-bipyridine)] (RuN3)-sensitized nanocrystalline TiO_2 thin films, can achieve a solar-to-electric power conversion efficiency of about 10% [7,21].

A cartoon of photoinduced electron transfer in molecule-semiconductor composites is shown in Scheme 1. Typically, the system can be described as a donor–bridge–acceptor unit with a chromophore (electron donor) anchored on the surface of semiconductor nanoparticle (electron acceptor) through a molecular spacer and anchoring group (bridge). Optical excitation of the chromophore to its excited states initiates electron injection (forward ET) from the molecular excited states into the semiconductor conduction band via the mediating bridge. The injected electron can recombine with the adsorbate cation (back ET), in competition with electron relaxation and diffusion processes in and between the nanoparticles.

Fundamentally, the injection process involves electron transfer between a discrete molecular state and a continuum of delocalized bulk states. Although the semiconductor states also become discrete when the particle size approaches the quantum-confined regime [22–28], the effect of this on ET rate has not been extensively studied. If the ET process is slower than intramolecular relaxation within the excited state manifold, then the optical excitation process need not be considered explicitly in understanding this problem. However, as we will discuss later, it is common for interfacial ET to occur on the time scale of vibrational relaxation (VR) and internal vibrational energy redistribution (IVR), necessitating consideration of competition between ET and intramolecular relaxation pathways.

Unlike its homogeneous counterpart [29–31], a detailed understanding of interfacial electron transfer is still lacking because of experimental, theoretical and computational difficulties. In addition to practical importance in device applications, semiconductor nanoparticles form non-scattering media with large surface area, enabling direct measurement of interfacial electron transfer rate [2–6] as well as other properties [5,22,26,32–41] using transient absorption or fluorescence techniques. In recent years, many research groups have investigated the dependences of electron transfer rate on the donor, spacer, anchoring group and semiconductor nanoparticles. In this article, we review our recent work in understanding photoinduced electron transfer from Ru and Re polypyridyl complexes to metal oxide nanocrystalline thin films. Related works by other groups will only be briefly discussed, since more in-depth reviews can be found in other contributions of this special issue. Readers are referred to earlier reviews for works prior to 1995 [2–4,42]. The rest of the article is organized as follows. The theoretical background for interfacial electron transfer is introduced in Section 2. Experimental details are described in Section 3. Competition of ultrafast electron injection and intramolecular relaxation process is discussed in Section 4. Section 5 summarizes our study of the dependence of injection rate on electronic coupling. The dependence of injection on relative energetics of adsorbate and semiconductor is discussed in Section 6. A summary and future outlook is presented in the final section.

2. Theoretical model of ET from adsorbate to semiconductor

Electron transfer between molecular adsorbates and bulk semiconductors (or metals) involves electron transfer between discrete molecular states and a dense manifold of highly delocalized electronic levels in the solid. The basic theoretical framework for describing electron transfer in bulk solid/liquid interfaces was developed by Marcus [43], Gerischer [44], and Levich and Dogonadeze [45] in

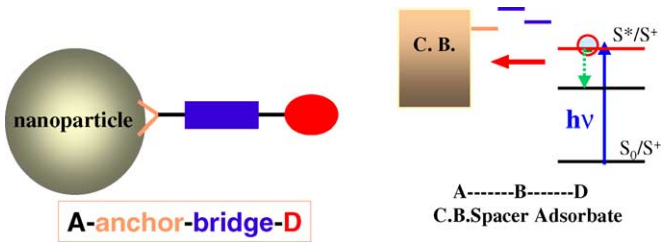

Scheme 1. Photoinduced electron transfer from molecules to semiconductor nanoparticles. A cartoon of a molecule donor–bridge–anchor–nanoparticle acceptor complex is shown on the left panel and the corresponding energetics on the right panel.

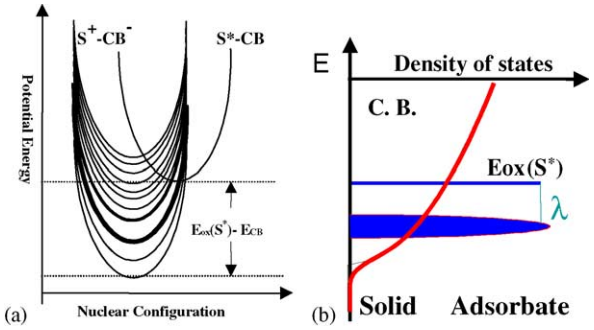

Scheme 2. (a) Marcus picture of interfacial electron injection. ET occurs from a reactant state to a continuum of product states, corresponding to different *k* states in the semiconductor. In the nonadiabatic limit, the total rate is a sum of ET to all possible states. (b) Schematic illustration of the dependence of total ET rate on semiconductor density of states and the reorganization energy.

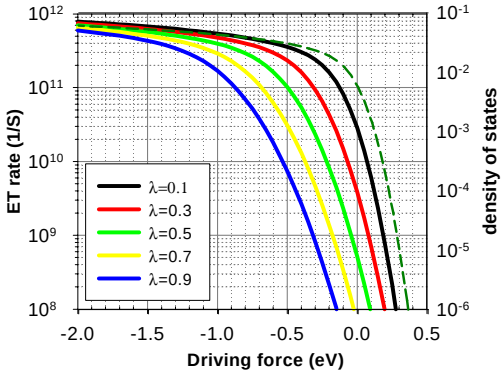

Fig. 1. Calculated density of states (dashed curve) of and electron transfer rate (solid curves) to SnO_2 as a function of driving force (difference between excited state potential and band edge) under different reorganization energy according to Eq. (1).

the 1960s. For photo-induced electron injection from adsorbate excited state to semiconductor, shown in Scheme 2, the reactant-state corresponds to the electron in the excited state of the dye and the product states correspond to the electron in the semiconductor conduction band. The discrete reactant state connects to a continuum of product states, each corresponding to the injected electron at a different electronic level in the semiconductor.

The ET rate to a state in the semiconductor depends on its electronic coupling with the donor orbital and molecular Franck–Condon overlap weighted density of states. Due to the existence of a continuum of accepting states in the semiconductor, interference of different reaction pathways presents a nontrivial problem in the strong coupling limit [46–48]. In the nonadiabatic limit, the total ET rate can be expressed as the sum of ET rates to all possible accepting states in the semiconductor [43,46–48]. Adopting an approach similar to Marcus and co-workers [46–48], the total ET rate from adsorbate to semiconductor is given by:

$$k_{\mathrm{ET}} = \frac{2\pi}{\hbar}\int \mathrm{d}E\rho(E)(1 - f(E, E_{\mathrm{F}}))|\bar{H}(E)|^2 \frac{1}{\sqrt{4\pi\lambda k_{\mathrm{B}}T}} \exp\left[-\frac{(\lambda + \Delta G_0 + E)^2}{4\lambda k_{\mathrm{B}}T}\right] \quad (1)$$

In equation 1, $\Delta G_0 = E_{\mathrm{cb}} - E_{\mathrm{ox}}$ is the energy difference between the conduction band edge and the oxidation potential of adsorbate excited state; $\rho(E)$ the density of states at energy E relative to the conduction band edge, which can contain both bulk states and surface states. $\bar{H}(E)$ the average electronic coupling between the adsorbate excited state and different k states in the semiconductor at the same energy E; and λ the total reorganization energy. The Fermi occupancy factor, $f(E, E_{\mathrm{F}})$ assures that electron injection occurs only to unfilled states. For wide bandgap semiconductors under no external bias voltage, negligible electron population in the conduction band may be assumed prior to injection, allowing this factor to be omitted.

To obtain some insight into the qualitative behavior of ET rate, it is useful to evaluate Eq. (1) for some simple cases. For nanocrystalline semiconductors not in the quantum confined size regime, the electronic structure of the bulk material still applies, but there is a significant contribution from surface and defect states. For a defect-free semiconductor, the density of states near the band edge of a simple conduction band is described by [157]:

$$\rho_0(E)\mathrm{d}E = \frac{(2m^*)^{3/2}}{2\pi^2\hbar^3}\sqrt{E}\mathrm{d}E \quad (2)$$

where m^* is the effective mass of electrons in the conduction band. The existence of defects introduces states below the band edge. For metal oxide nanocrystalline thin films, an exponentially decaying defect state density below the band edge is often assumed [49,50] on the basis of photoelectrochemical measurements of carrier absorption and transport in thin film [51–54]. Assuming that the effective electronic coupling is independent of the energy, the injection rate, k_{ET}, as a function of $E_{\mathrm{cb}} - E_{\mathrm{ox}}(s^*)$ can be calculated as shown in Fig. 1. The injection rate increases when the adsorbate excited state is further above the conduction band edge (more negative value of $E_{\mathrm{cb}} - E_{\mathrm{ox}}(s^*)$). The change is small high above the band edge, but is nearly exponential near the band edge, reflecting the variation of conduction band density of states.

It should be noted that the dependence on density of states can be much more complicated than the simple case shown in Fig. 1. The ET rate depends on not the total density of states, but only on those coupled to the adsorbate electron donating orbital. The coupling strength likely varies for different band states (bulk versus surface, d versus sp bands). This point was illustrated in a recent computational study of nonadiabatic ET on metal surfaces [48]. Furthermore, there exists an inhomogeneous distribution of adsorbate/semiconductor interactions (crystal surfaces, adsorption site, adsorption geometry, etc.), giving rise to a distribution of electronic coupling matrix elements, H, and hence injection rates. Therefore, non-single exponential injection kinetics are to be expected [6,55,56].

Furthermore, the expression in Eq. (1) is only valid for the high temperature limit, although full quantum mechanical treatments of interfacial ET have also been reported [57–60]. Despite these limitations, this simple model does contain the basic features of interfacial ET and should serve as a good starting point to examine the qualitative dependence on ET rate on properties of semiconductor, adsorbate and the interfacial environment.

3. Experimental section

3.1. Techniques for studying interfacial ET

Much previous understanding of interfacial electron transfer was derived from cyclic voltammetry and chronoamperometry measurements in an electrochemical cell [1,2,61–76]. When interfacial electron transfer is the rate limiting step, a direct correspondence between current and ET rate can be obtained and ET rate can be readily derived [62,77,78]. These approaches have been used extensively and successfully for investigating slow electron transfer through self-assembled monolayers of alkanethiol or other chemical species on metal and semiconductor electrodes [65,66,69]. Indirect laser induced temperature jump technique has pushed the limit of this type of approach to a faster time scale [65,66], but for ultrafast electron transfer (<ns), time-resolved spectroscopy is needed [79].

The interfacial nature of these processes has hindered their direct time-resolved spectroscopy studies in the past. The study of dynamics on bulk surfaces often demands sophisticated surface science methods for samples in UHV chambers [80–87]. Efforts to develop in situ, direct and interface-specific spectroscopic techniques for studying bulk solid/liquid interfaces have resulted in some elegant yet complicated techniques, such as sum frequency (SFG) and second harmonic (SHG) generation [88–90], and surface restricted grating techniques [42].

Time-resolved fluorescence has long been used for measuring interfacial ET rate [91–96]. In these measurements, changes in fluorescence lifetime is measured, from which electron transfer rate is determined. With modern techniques, excellent time resolution (sub-100 fs) [97] and sensitivity (single molecule detection) [98,99] can be obtained. However, clear determination of charge transfer can sometimes be complicated by other fluorescence quenching pathways such as energy transfer between adsorbate molecules.

In recent years, transient absorption techniques have been widely used to directly measure electron transfer rate in nanomaterials. Colloidal particles, nanoporous films and other nanostructures are amenable to this type of study because they provide non-scattering media with large surface area (and hence high adsorbate concentration). Transient absorption spectroscopy provides the opportunity to directly interrogate charge transfer dynamics, since it allows spectroscopic identification of all the species (ground and excited states and oxidized and reduced forms) of the donor and acceptor present at a given time delay [100]. The technique may be used for charge transfers occurring over a wide range of timescales. Vast improvement in ultrafast laser technology has rendered transient absorption spectroscopy the most commonly used technique for investigating semiconductor/molecule electron transfer dynamics, particularly fast electron injection. There are two distinct types of transient absorption spectroscopy that are used, probing in the visible/near-IR and probing in the mid-IR.

Transient absorption spectroscopy in the visible/near-IR region has been used by many groups to study interfacial electron transfer [101–140]. This technique detects electronic transitions of the adsorbate in ground, excited and oxidized forms, as well as a small contribution from injected electrons in the semiconductor [111,117,120,121]. This technique affords excellent time resolution (substantially shorter than 100 fs is presently attainable, even allowing investigation of wavepacket motion during electron transfer) [112,135]. The primary drawback to the technique is spectral overlap between broad absorption bands of different states of the adsorbate (ground, singlets, triplets and oxidized form). As a result, it is often necessary to probe over a wide spectral range to separate the dynamics of different absorbing species [111,120,121]. Anisotropy of the signal can also be used to separate overlapping species with different transition dipole moment direction [120,121,123,124]. In some well-chosen dye molecules [117], clean separation of different absorbing species can be achieved.

Transient absorption spectroscopy probing in the mid-IR has also been used to study interfacial electron transfer in semiconductor nanoparticles [6,55,56,141–156]. The technique probes the vibrational transitions of the adsorbate in ground, excited and oxidized forms, as well as strong IR absorption of injected electrons in the semiconductor [149]. The IR absorption of electrons results from free carrier absorption, intrasubband transitions and trap absorption [157]. It has been used to study carrier dynamics in semiconductor quantum dots [23,37,158–161]. For free carrier absorption, scattering with phonons is also required for momentum conservation, leading to an absorption coefficient that increases as a power (generally 2–4) of the wavelength [157]. Its absorption coefficient is strong in the mid-IR and becomes negligible in the visible region. Because the electron signal is present in all semiconductors, this technique can be used to study any adsorbate/semiconductor composite. The IR absorption signal of electrons depends on both the population and absorption strength of the injected electrons. The latter depends on the energetics of the electron and its change reflects relaxation dynamics. Relaxation dynamics can be separated from electron population change by monitoring the dye vibrational spectrum or electronic absorption in addition to IR absorption of electrons [143,148]. They can also be independently determined in an IR-pump/IR-probe measurement of electrons.

3.2. Femtosecond tunable spectrometer

The tunable femtosecond infrared spectrometer used for our studies was based on a regeneratively amplified femtosecond Ti:Sapphire laser system (1 kHz repetition rate at 800 nm, 100 fs, 900 μJ/pulse) and nonlinear frequency mixing techniques. A detailed description of this setup has been presented previously [149,154].

The 800 nm output pulse from the regenerative amplifier was split into two parts to generate pump and probe pulses. One part, with 300 μJ/pulse, was frequency doubled and tripled in BBO crystals to generate pump pulses at 800, 400 or 267 nm, or alternatively, to pump an optical parametric amplifier (OPA) to generate tunable pulses in the visible. The remaining 600 μJ of the 800 nm pulse was used to pump a Clark IR-OPA to generate two tunable near IR pulses from 1.1 to 2.5 μm. These signal and idler pulses were combined in an $AgGaS_2$ crystal to produce mid-IR pulses tunable from 3 to 10 μm by difference frequency generation. When desired, visible probe pulses were generated using continuum generation by focusing the fundamental into a sapphire window.

The mid-infrared probe pulse was spectrally dispersed using an imaging spectrograph and imaged onto a 32 element infrared HgCdTe(MCT) array detector [149]. The amplified outputs of the 32 elements were measured for every laser shot at a 1 kHz repetition rate. Each element of the array averaged a 5 cm^{-1} slice of the infrared spectrum so that the total spectral region covered by the array was about 160 cm^{-1}. When necessary, a more dispersive grating was used to obtain better spectral resolution. To minimize low frequency laser fluctuations, the main noise source, every other pump pulse was blocked with a synchronized chopper (New Focus model 3500) at 500 Hz, and the absorbance change was calculated with two adjacent probe pulses (pump blocked and pump unblocked). Transient kinetics at 32 wavelengths were collected simultaneously, from which transient spectra at different delay times were constructed.

The zero delay time and instrument response for a 400 nm pump/mid-IR probe experiment were determined using a thin silicon wafer or thin film of CdS nanoparticles, in which absorption of 400 nm photons leads to the instantaneous generation of charge carriers that absorb strongly in the mid IR region [157]. The typical instrument response, which was determined in every experiment, could be well represented by a Gaussian function with FWHM ranging from 150 to 320 fs.

3.3. Materials

Synthesis of nanoparticles and preparation of thin films were carried out according to published procedures. We will only describe briefly the preparation of RuN3 dye-sensitized nanocrystalline TiO_2 thin films. Similar procedures were used to prepare films of other semiconductor materials and sensitizer molecules [21,149,152,155,162].

The TiO_2 nanocrystalline thin films were prepared by a method similar to that used by Zaban and co-workers [163]. Briefly, the TiO_2 nanoparticle colloid was synthesized by the controlled hydrolysis of titanium(IV) isopropoxide in a mixture of glacial acetic acid and water at 0 °C. The resulting solution was heated to 80 °C for 8 h and then autoclaved at 230 °C for 12 h. The resulting colloid was concentrated to 150 g/L and spread onto polished sapphire windows and baked at 400 °C for 36 min. Immersion and storage of the TiO_2 films in a room temperature ethanol solution containing 200 μM Ru535 and 20 mM chenodeoxycholic acid resulted in adsorption of the RuN3 to the porous film surface.

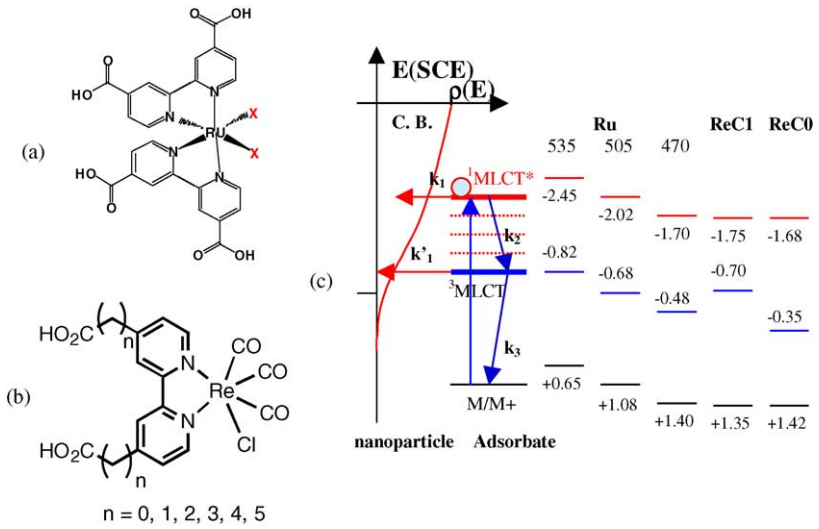

Scheme 3. Schematic structures of (a) Ru535 (2X = 2NCS$^-$), Ru505 (X = CN$^-$) and Ru470 (2X = dcbpy) and (b) ReCn (n = 0–5) and (c) schematic illustration of two-state injection model. Electron injection (k_1) from unthermalized excited state competes with intramolecular relaxation (k_2) and the relaxed state injects with a rate constant k'_1. The competition leads to biphasic injection kinetics (see Eq. (4) in main text). The oxidation potentials for the ground, excited state (unrelaxed and relaxed) of dyes are shown to the right. Oxidation potentials are adopted from a [132], b [170], and d [171]; and c estimated to be 200 meV less than Ru505 [170]. Values for the ^{1}MLCT* state are calculated based on excitation by a 400 nm photon (3.1 eV).

The amount of dye coverage was controlled by the immersion time. High purity $Ru(dcbpy)_2(X)_2$ [X_2 = 2SCN (called RuN3 or Ru535), 2CN (Ru505), and dcbpy (Ru470)] compounds, shown in Scheme 3, were purchased from Solaronix (Lausanne, Switzerland). $Re(dcbpyCn)(CO)_3(Cl)$ [called ReCn, dcbpy Cn = 2-2′-bipyridine-4,4′-$(CH_2)_n$–COOH, n = 0–5] were synthesized in our and collaborator's laboratories [56,144,164]. During the experiment, thin films were either exposed to air in ambient conditions or submerged in a solution. Film samples were moved rapidly during measurement to avoid long-term photoproduct buildup.

4. Competition between electron injection and molecular relaxation processes

4.1. Two-state injection model

Many groups have reported biphasic electron injection kinetics from Ru535 to TiO_2 with a < 100 fs fast component and slower ps components [6,105,108,111,116, 119–121,132,143,146,151,152]. Similar ultrafast injection on the 100 fs or less time scale has been reported for many organic dyes [91,117,153] and other Ru and Re polypyridyl complexes (Scheme 3) [6,132,143,146]. The rapidity of charge transfer suggests the importance of injection from vibrationally and electronically unrelaxed excited states. In recent years, advances in ultrafast spectroscopy have facilitated numerous experiments that have clearly demonstrated competition between injection and adsorbate intramolecular relaxation [56,112,120,121,139,143]. For example, Willig and co-workers observed that in perylene/TiO_2, the motion of the wave packet in the neutral excited state generated by fs excitation continued in the ionized adsorbate, providing clear evidence of electron transfer from an unrelaxed vibrational population and prior to vibrational dephasing [112]. Our recent study of study of $Re(dcbpy)(CO)_3Cl$ (ReC0)/TiO_2 also showed injection occurred prior to vibrational relaxation of adsorbate and produced hot electrons in the semiconductor (see discussion below) [56,143].

For the Ru and Re polypyridyl complexes, photoexcitation prepares a ^{1}MLCT state with a manifold of ^{3}MLCT states lying substantially lower in energy [165]. As shown in Scheme 3, at 400 nm excitation, the energy difference between the initially excited single state and the relaxed triplet state ranges from 1.0 to 1.6 eV. Intersystem crossing and relaxation within the excited state manifold has been shown to occur on the <100 fs time scale in related $Ru(bpy)_3$ due to strong spin-orbit coupling [166–169]. For RuN3/TiO_2, transient absorption and stimulated emission measurements showed that ISC occurs on a 75 fs timescale while ET from the ^{1}MLCT state occurs on a 50 fs timescale [120].

We have proposed a two-state injection model (Scheme 3c) to account for the competition between adsorbate relaxation and electron injection processes [6,143, 146]. Similar models have been used by other groups [120,121,139]. In this model, photoexcitation of the adsorbate prepares an unrelaxed excited state (^{1}MLCT*), from which it can undergo electron injection to semiconductor with a rate constant of k_1, or relaxation in the excited state manifold with a rate constant of k_2. The latter includes both intersystem crossing and subsequent vibrational relaxation. Electron injection can also occur from the relaxed state with a rate constant of k_1'. When the potential for the relaxed excited state is near the conduction band edge and significantly lower than that of the unrelaxed state, k_1' is expected to be significantly slower than k_1 due to a rapid decrease in density of conduction band states near the band edge. Assuming $k_1' \ll k_1, k_2$, the injection kinetics are given by [143]:

$$N_e(t) = N_0 \left[\frac{k_1}{k_1 + k_2}(1 - e^{-(k_1+k_2)t}) + \frac{k_2}{k_1 + k_2}(1 - e^{-k_1' t}) \right] \quad (3)$$

where N_e(t) is the time dependent population of injected electrons and N_0 the population of the initially excited molecules.

Eq. (3) predicts biphasic injection kinetics, consisting of a fast component with rate constant $k_1 + k_2$ and a slower component with rate constant k_1'. Since k_2 is on the order of 1/75 fs [120], the fast component will have a <100 fs rise time regardless of the injection time. Therefore, variations in k_1 may not be apparent in the rise time of the fast component, if the instrument response time of a pump probe measurement is over 100 fs. However, the amplitude of the observed fast injection is determined by ratio of the rate constants k_1/k_2, which may serve as a more sensitive indication of k_1.

The model predicts two extreme cases. In the case that electron injection from unthermalized state is much slower than intramolecular relaxation, $k_1 \ll k_2$, the fast injection component is negligible and injection is dominated by the slow components.

$$N_e(t) = N_0(1 - e^{-k_1' t}) \quad (4)$$

In this case, the photoexcited molecule undergoes relaxation within the excited states before electron injection, a notion that was commonly accepted before recent observation of injection from unrelaxed excited states. On the other extreme, when injection from the relaxed state is not energetically favorable, the fast component dominates injection kinetics.

$$N_e(t) = N_0 \frac{k_1}{k_1 + k_2}(1 - e^{-(k_1+k_2)t}) \quad (5)$$

4.2. Injection from the relaxed excited state

Selecting a molecule with reduced injection rate from the initially populated state should decrease the amplitude of the fast injection component and lead to kinetics dominated by slow components. ReCn ($n \geq 1$, see Scheme 3) serve as examples of this case [56,143]. For ReC1 and ReC3 sensitized TiO_2, we observed only slow injection component,

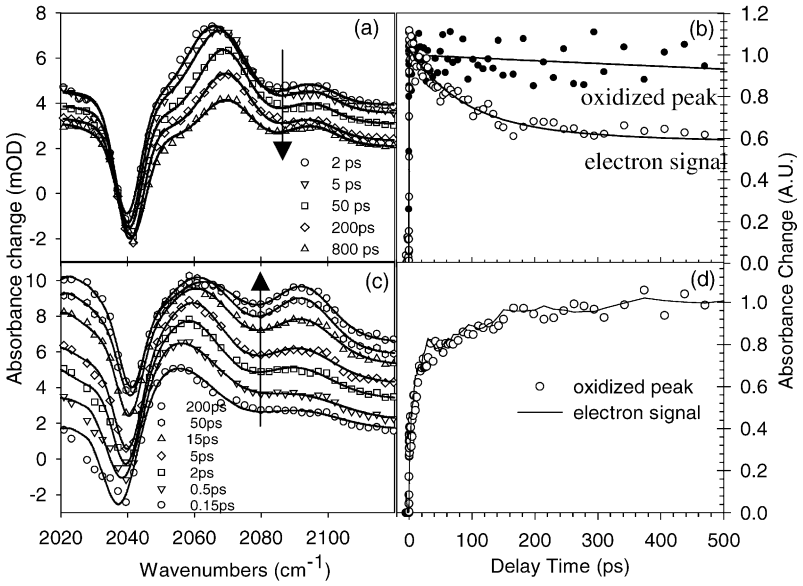

Fig. 2. Comparison of electron injection dynamics from ReC0 and ReC1 into TiO_2 nanocrystalline thin films. (a) Transient spectra of ReC0 CO stretching mode and broad IR absorption of injected electrons as a function delay time after 400 nm excitation. The peaks at 2040, 2060 and 2090 are assigned to ground, excited and oxidized form of ReC0, respectively. (b) Comparison of kinetics probed by IR absorption of injected electron absorption (open circles) and CO stretching band intensity of oxidized adsorbate (full circles). The oxidized peak trace shows <50 fs electron injection and negligible subsequent change within 1 ns. The decrease of the IR absorption of injected electrons is attributed to the relaxation of injected hot electrons in TiO_2. Analogous transient spectra and kinetics for ReC1/TiO_2 are shown in (c) and (d) (reproduced with permission from J. Phys. Chem. B, 2000, 104, 11957–11964 and [143], Copyright 2000 and 2003 American Chemical Society).

characterized by a 20 and 190 ps stretched exponential rise [56]. The slower injection rate can be attributed to the reduced electronic coupling introduced by the addition of CH_2 groups between the bipyridine and the carboxylate anchoring group.

Injection dynamics from ReC1 to TiO_2 are shown in Fig. 2c and d. The peaks at 2040, 2060 and 2090 in the transient spectra (panel c) are assigned to the ReC1 ground, excited and oxidized form, respectively. The spectra are fitted with Gaussian line shapes (solid line) from which the integrated area of the oxidized peak (at 2090 cm^{-1}) is calculated to obtain the population of injected electrons. Shown in frame d is a comparison of the magnitude of the oxidized peak and the IR absorption of electrons, showing identical traces for these signals. The amplitude of the fast (<100 fs) injection component is negligible. The kinetics are dominated by a slow stretched exponential rise with a time constant of about 20 ps, suggesting that injection occurs from its relaxed ^{3}MLCT state at −0.7 V (SCE), near the conduction band edge [56]. Its slow rate can be attributed to the reduced electronic coupling strength resulting from the CH_2 spacer group, as well as to the lower density of accepting states near the band edge.

4.3. Injection from the unrelaxed excited state

Selecting an adsorbate with relaxed ^{3}MLCT state substantially below the band edge suppresses the slow component and results in injection that is dominated by fast injection from the unrelaxed excited state. ReC0 on dry TiO_2 film is an example of this case [56,143,146]. The ReC0 relaxed excited state is estimated to be at −0.35 V (SCE). The band edge of TiO_2 of a dry film is not known but expected to be more negative than −0.5 V, its position at pH 2.

Injection dynamics from ReC0 to TiO_2 are shown in Fig. 2a and b. Similar to ReC1, the peaks at 2040, 2060 and 2090 in the transient spectra (panel a) are assigned to ReC0 ground, excited and oxidized form, respectively. The injection dynamics are very different. As shown in Fig. 2b, the oxidized peak is formed within the instrument response limit and shows negligible subsequent change, indicating an apparent rise time of <50 fs and no slow injection components. The lack of slow component indicates that in this system, injection from the relaxed state does not occur on the <1 ns time scale, consistent with the low density of accepting states for injection from the relaxed excited state. The electron signal, which is also formed within 50 fs, shows a decay on the 100 ps time scale that was not observed in ReC1. This decay is attributed to the relaxation of hot electrons injected high above the band edge [143]. Similar hot electron relaxation has also been demonstrated in molecule-to-nanoparticle CT complexes, $Fe(CN)_6/TiO_2$, in which photoexcitation of the CT band injects an electron instantaneously to a TiO_2 state high above the band edge [143,148,154]. A shift of excited state CO stretching peak on the few ps time scale was also observed in Fig. 2a and can be attributed to the vibrational relaxation of the hot excited molecule [6,149]. The <50 fs rise of electron signal in ReC0 demonstrated that the fast in-

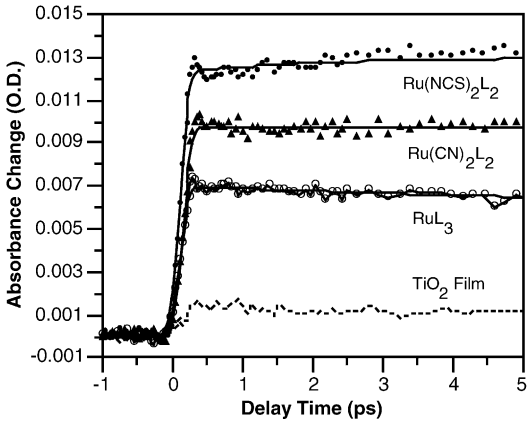

Fig. 3. Comparison of electron injection kinetics in Ru535, Ru505 and Ru470 sensitized TiO_2 thin films measured at 2045 cm^{-1} after 400 nm excitation. All samples have same OD at 400 nm and were measured under the same laser conditions. The amplitude of the fast component decreases from Ru535 to 470. Also shown as a dotted line is the signal from an unsensitized film under the same excitation power (reproduced with permission from [6], Copyright 2001 American Chemical Society).

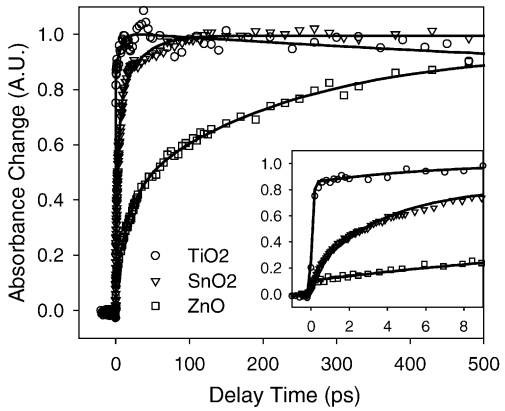

Fig. 4. Comparison of electron injection dynamics from Ru535 to TiO_2, SnO_2 and ZnO. All samples were excited at 400 nm and probed at 2000 cm^{-1}. The inset shows the same data on a shorter time scale. Injection kinetics are biphasic in all systems, although the amount of fast component and the rate of slow component differ.

jection occurred prior to vibrational energy relaxation in the excited state.

4.4. Biphasic injection

For the Ru polypyridyl complexes shown in Scheme 3, the relaxed ^{3}MLCT states are near the band edge of TiO_2 and the Franck–Condon states at 400 nm excitation are about 1 V higher. For these systems on TiO_2, the two-state injection model predicts biphasic injection kinetics. In addition to Ru535 [6,105,108,111,116,119–121,132,143,146,151,152], biphasic injection in other Ru complexes to TiO_2 have also been observed [6,143,146]. A comparison of injection kinetics from Ru535, Ru505, Ru470 to TiO_2 is shown in Fig. 3. A < 100 fs injection component was observed for all dyes but the amplitude of fast component and the rates of slow components vary. These films have the same optical density at 400 nm, corresponding to the same number of absorbed photons. The comparison indicates that the amplitude of the fast component decreases and the rate of slow component becomes slower, correlating with the decreasing potential (less negative) of ^{1}MLCT and ^{3}MLCT excited states in these compounds. As will be discussed in the next section, a less negative potential leads to a decrease of k_1 and k_1' because of the reduced density of accepting states in TiO_2. A similar trend has also been observed for these three complexes on TiO_2 in pH 2 buffer [143].

Biphasic injection to other semiconductor nanoparticles has also been observed [6,55,119,137,139,156]. Shown in Fig. 4 is a comparison of injection dynamics (probed at 2000 cm^{-1}) from Ru535 to TiO_2, ZnO and SnO_2 after 400 nm excitation. Electron injection kinetics to all three semiconductors are biphasic, consisting of a fast (<100 fs) component and slower components. The amplitude of fast component is 60% (after correction for cross-section decay of hot electrons [143]) for TiO_2, 15% for SnO_2 and <15% for ZnO. The slow injection component is non-exponential in all three semiconductors. The average time constant is 150 ps in ZnO, 10 ps in SnO_2, and 9–20 ps for TiO_2 films (under different conditions) [108,121,143]. The relative value of rate constant k_1 can be determined from the amplitude of fast component using Eq. (3). Assuming that the intramolecular relaxation rate, k_2, is independent of the substrate, we estimate >10 times faster k_1 for TiO_2 than ZnO.

Different injection rates to these semiconductors may be caused by differences in band structure, electronic coupling strength and density of semiconductor states [46,47]. The TiO_2 conduction band is composed primarily of empty 3d orbitals of Ti^{4+} [172–174], while the ZnO conduction bands are largely derived from empty s and p orbitals of Zn^{2+} [173]. One effect of the different band structures is a higher density of states in TiO_2. From the effective mass of the conduction band electron in TiO_2 (5–10 m_e) and ZnO (0.3 m_e) [175,176], the density of conduction band states near the band edge is predicted to be as much as two orders of magnitude higher in TiO_2 [176]. Another possible factor is the electronic coupling between the dye excited state (donor) and conduction band (acceptor). Clearly, a more quantitative comparison of injection rates in different semiconductors needs to consider both factors, which likely requires high level quantum chemical calculation of electronic coupling strength and relevant density of states in semiconductor.

Direct spectroscopic evidence for distinct singlet and triplet electron injection pathways have been obtained for Ru polypyridyl complexes on SnO_2 [139] and TiO_2 [120,121]. In these studies, stimulated emission from the singlet state was observed, providing a direct measure of the reduction of singlet lifetime caused by electron injection pathway. In the detailed study of Ru535/TiO_2 by Sundstrom and coworkers [120,121] transient spectral evolution from 400 to 1000 nm was observed to clearly resolve absorption bands of the ground, excited, and oxidized form, as well as injected

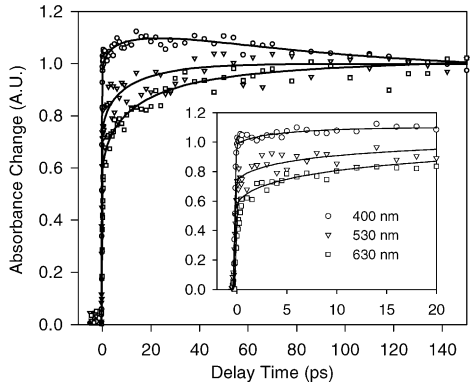

Fig. 5. Normalized comparison of electron absorption dynamics of Ru535-sensitized TiO_2 films in ethylene/propylene carbonates (1:1) after excitation at different wavelengths. Inset: the same data plotted on a shorter time scale. The solid lines are fits using the two-state injection model. The fast component is well described by a <100 fs rise and the slow component is fit by a stretched exponential function with a 50 ps time constant (reproduced with permission from [143], Copyright 2003 American Chemical Society).

electrons. With 30 fs laser pulses, stimulated emission of singlet state and formation times of triplet state and cation were directly measured, showing biphasic injection attributable to injection from singlet and triplet states.

Other studies of metal polypyridyl-sensitized metal oxides have suggested the broader applicability of the two-state injection model. For example, comparison of ruthenium polypyridyl complexes on TiO_2 with their osmium counterparts demonstrated that the fast injection had larger relative amplitude for the ruthenium complexes [132]. This suggests a decrease of the ratio k_1/k_2 for the osmium complexes, a prediction that may be rationalized on the basis of increased spin-orbit coupling relative to the ruthenium complexes [177]. The faster k_2 for the osmium complexes thus reduces fast injection. Biphasic injection kinetics were also observed on SnO_2 for Ru470 [139], Ru535 [6,119], and other Ru derivatives [6].

4.5. Dependence on excitation wavelength

To provide further support for injection from unthermalized excited states, we studied the excitation wavelength dependence of injection dynamics from RuN3 to TiO_2. If the fast component of electron injection occurs from the unrelaxed excited state, then by varying the excitation wavelength (the energy of the hot excited state), we should be able to control the partitioning between the fast and slow injection components.

The measured transient IR absorption kinetics of Ru535-sensitized TiO_2 films soaked in an 1:1 ethylene/propylene carbonate mixture (referred to as EC/PC) are shown in Fig. 5. The main panel shows the kinetics traces that correspond to 400 nm (open circles), 530 nm (open triangles) and 630 nm (open squares) excitation wavelengths. These kinetics traces have been normalized to have the same signal magnitude at 150 ps. The inset to the figure shows the same data plotted on a shorter time scale. The kinetics are well described by a fast (<100 fs) injection component with cross-section decay and slow component on the 50 ps time scale [143]. Clearly, the contribution of the fast injection component decreases at longer excitation wavelengths. By increasing the excitation wavelength, we prepare the unrelaxed state at closer energy to the conduction band edge. As a result, the density of electron accepting states in TiO_2 decreases, which reduces the electron injection rate from the unthermalized state, k_1. The smaller energy difference between the relaxed and unrelaxed state may also increase the rate of relaxation out of the fast injection region, k_2. Both factors lead to a decrease of the amplitude of the fast injection component. This trend was also observed by other groups for Ru535/TiO_2 [120,121,132,143]. We have also recently observed similar wavelength dependence of the fast injection component for Ru535/ZnO [156].

Evidence for injection from unrelaxed excited state was also observed by microsecond time resolved spectroscopy of dye sensitized films [178–182]. On the microsecond time scale, all photoexcited Ru535 molecules or derivatives have either formed cations through electron injection or returned to ground state, while no significant back ET has occurred yet [178–182]. The amplitude of ground state bleach (or cation absorption) of the sensitizer reflects the quantum yield of electron injection. Using this approach, it was found that electron injection yield for Ru535 on Nb_2O_5 decreases at longer excitation wavelength while that on TiO_2 does not [178,179]. It indicates that for Nb_2O_5, injection occurs only through the unrelaxed excited state, which is consistent with its higher band edge position than TiO_2. Meyer and coworkers [180–182] have shown that the injection quantum yield depends on the cation and proton concentrations in the sample, which affects the band edge position. These indirect measurements are consistent with wavelength and pH dependent injection kinetics directly resolved using femtosecond lasers [120,121,143]. Electron injection from the unrelaxed state has also been used to explain wavelength dependent absorbed-photon-to-current conversion efficiency measured in solar cells [183,184]. Ferrere and Gregg [184] observed that in an $Fe(dcbpy)_2(CN)_2$ sensitized TiO_2 solar cell, the photocurrent action spectrum differs from the absorption spectrum of the sensitizer showing higher conversion efficiency in higher energy absorption bands. In this case, the relaxed (lowest) excited state is a ligand field state below the band edge, from which electron injection is not likely and only injection from the unrelaxed state is possible. The observation of photocurrent indicates that injection occurs from unrelaxed excited states and its band selectivity reflects the dependence of injection kinetics on excitation wavelength, as predicted by the two-state model and observed for RuN3/TiO_2 [143].

It should be noted the two-state injection model is the simplest model that can take into account the competition of intramolecular relaxation and electron injection pathways. A more complete model should include injection from all possible states between the initially prepared ^{1}MLCT Frank–Condon state and final relaxed ^{3}MLCT state. Despite

the simplifications, the two-state electron injection model appears to be a useful tool for describing electron injection from metal polypyridyl complexes to semiconductor nanoparticles. This model emphasizes the importance of separating injection from the non-thermalized and thermalized excited states in comparing electron injection rates. Due to the fast intramolecular relaxation and generally slower injection from the relaxed state in metal polypyridyl complexes, separation of timescales is usually possible and necessary. In systems with slower intramolecular relaxation processes and smaller difference between thermalized and unthermalized states, the separation of time scales become difficult and the two-state model may no longer be adequate.

5. Dependence on electronic coupling

A well-established method of modifying coupling between adsorbate and semiconductor is the insertion of bridging units between the chromophore and the binding group [64–76]. In principle, introduction of successive numbers of units allows a systematic investigation of the dependence of ET rate on bridge length. Many studies of this type have been performed for slower electron transfer reactions, particularly exploring electron transfer through self-assembled-monolayer on metal [65,66] or semiconductor electrodes [69,70]. These studies have shown that electron transfer rate for longer bridges ($r > 10$ Å) generally varies exponentially with the length of the bridge r [65,66]:

$$k_{ET}(r) = k_0 e^{-\beta_r r} \quad (6)$$

where k_0 is the extrapolated rate constant for $r = 0$, and β_r the exponential decay coefficient. For bridges with repeat spacer units, the exponential dependence can also be expressed in terms of the number of spacer units and a corresponding coefficient β_n.

Theoretical studies predict the dependence of coupling on the number of spacers in short alkyl chains to deviate from exponential [30,185–188] and to oscillate between odd and even n [189,190]. This behavior is expected to be general for bridge assisted electron transfer processes [30,191]. Indeed, the odd-even effect in ET rates has been observed in some methylene bridged molecular donor–acceptor complexes in solution, [192] but not all [193–196]. For interfacial ET, this phenomenon is even less well understood. In a recent study of ET through short chain ($n = 2$–8) alkanethiol self-assembled-monolayers (SAMs), the n dependence was found to level off at $n = 2$, which was attributed to the solvent viscosity dependence of ET in the adiabatic regime [197]. Similar reduction of distance dependence at even longer distance has also been observed for alkanethiol [65,66] and oligophenylenevinylene bridges [198].

To study electron transfer in the strong coupling limit, direct time resolved techniques are needed. Using femtosecond time-resolved infrared spectroscopy, we investigated electron injection from a rhenium complex with $n = 0$–5 methylene groups inserted between the bipyridine ligand and the carboxylate binding group. Reduction of injection rate with bridge distance was observed in a subset of these adsorbates ($n = 0$, 1, 3) on TiO_2 [56]. More recently, we examined the distance dependence of electron injection rate from the complete series of adsorbates to SnO_2 [144]. As shown in Fig. 6a, a decrease of injection rate with increasing number of methylene spacer units was clearly observed. A plot of average rate constant versus number of spacer units is shown in Fig. 6b. Exponential rate decrease with $\beta_n = 1$, congruent with that seen for long bridges [65,66], was observed extending down to $n = 3$. For $n = 2$ and $n = 1$, similar rates (1/40 ps) were obtained. The reason for deviation from exponential dependence at $n < 3$ remains to be further investigated.

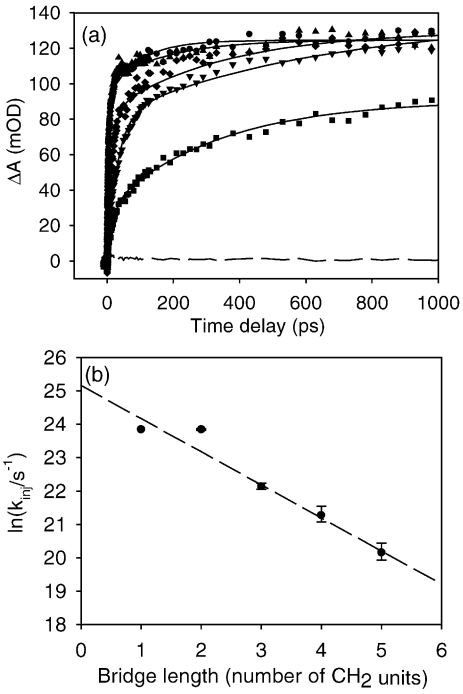

Fig. 6. Comparison of electron injection from ReCn ($n = 1$–5) to SnO_2 film at pH 2. (a) Injected electron traces probing at 2120–2150 cm^{-1} for ReC1 (circles), ReC2 (triangles), ReC3 (diamonds), ReC4 (inverted triangles), and ReC5 (squares). The solid lines are two-exponential fits to the data. The dashed line is the signal from an unsensitized SnO_2 film, which has already been subtracted from the other traces. (b) Plot of the natural logarithm of injection rate versus number of methylene bridging groups. The relative rates (with respect to ReC1/SnO_2) were determined using the time scaling technique described in [144]. The absolute rate was then obtained by multiplying these scaling factors by the ReC1 τ_{eff} = 44 ps from the two exponential fit. ReC1 and ReC2 exhibited nearly identical rates, but ReC3 to ReC5 show a linear trend, with $\beta_n = 0.99$ (reproduced with permission from [144], Copyright 2003, American Chemical Society).

ET through short conjugated bridges has also been investigated. Kilsa utilized 0–2 xylyl bridging groups for a ruthenium terpyridine dye on TiO_2 [133]. Unfortunately, the injection step was not clearly resolved and the distance dependence of injection rate remains unclear. Very little distance dependence was observed in the back ET process.

Some uncertainty may be introduced into these studies of bridge-dependent coupling by flexibility of the bridge and/or variations in binding geometry. Recently Galoppini and coworkers [140,199–201] have developed a tripodal adsorbate, with rigid bridge, to help avoid these uncertainties. This anchoring may prove extremely useful in eliminating unwanted factors from investigation of coupling-dependent electron injection. Although a systematic study of bridge-length dependence has not yet been performed on this system, a preliminary study indicates ultrafast injection over long distance [140].

Another method of modifying coupling between adsorbate and semiconductor is by changing the binding group on the adsorbate. Many linkages (phosphonate, carboxylate, acetylacetonate, etc.) have been successfully used to bind adsorbates to TiO_2 [7,202–204] However, relatively few studies have yet investigated the dependence of injection rate on binding groups. Our recent study shows that there is significant difference in injection rate to SnO_2 from ReC1 complexes with –COOH, $–PO_3H_2$ and –SH anchoring groups [205].

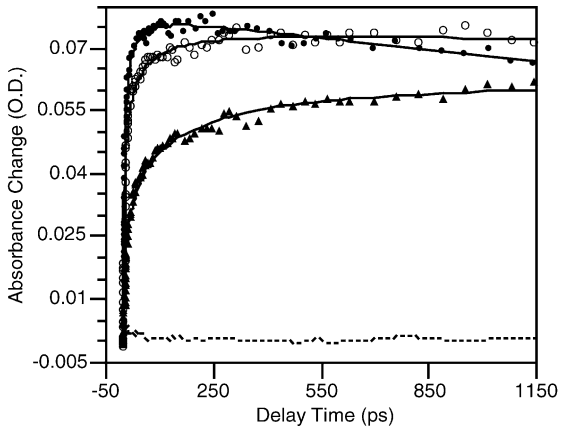

Fig. 7. Comparison of electron injection kinetics in $Ru(dcbpy)_2X_2$ [X_2 = $2SCN^-$ (full circles), $2CN^-$, (open circles) and dcbpy (full triangles)] sensitized SnO_2 thin film measured at 2088 cm^{-1} after 400 nm excitation. Solid curves are stretched exponential fits to the data. The signal from an unsensitized film under the same excitation power is shown as the dotted line (reproduced with permission from [6], Copyright 2001 American Chemical Society).

6. Density of accepting states

Eq. (1) suggests that in the nonadiabatic limit, injection rate depends on the density of electron accepting states in the semiconductor. As illustrated in Scheme 2, near the conduction band edge, the density of states increases at higher energy, leading to a higher density of accepting states for injection from an adsorbate with more negative oxidation potential, As a result, faster injection is predicted for a larger difference between the adsorbate excited state potential and conduction band edge, as shown in Fig. 1.

One method of tuning the relative energetics is changing the adsorbate excited state oxidation potential. A systematic trend is observed when comparing electron injection from Ru535, 505 and 470 to TiO_2 [143] or SnO_2 [6]. These dyes are attached to the semiconductor through the dcbpy ligand, but they differ in the third pair of coordination ligands, which leads to lowering of ground and excited state oxidation potential from Ru535, to 505, to 470, as shown in Scheme 3. Injection kinetics from these dyes to TiO_2 films were compared previously [6,143] and are shown in Fig. 3. The amplitude of fast component and rate of slow component become smaller, consistent with the trend of their decreasing excited potentials and corresponding density of electron accepting states in TiO_2. This trend is even more clearly demonstrated for these dyes on SnO_2 film, shown in Fig. 7. In this case, electron injection is dominated by slow components and the rates become slower from Ru535 to Ru470. While the observed trend is consistent with change of adsorbate energetics, it is unclear whether there is significant difference in electronic coupling among these adsorbates.

An alternative approach is modifying the conduction band edge energy by varying pH or potential-determining ion concentration. Changing the sample pH affects a Nernstian-type change in the semiconductor band edge position for metal-oxide semiconductors [44,206–208]:

$$V(\mathrm{pH}) = V(\mathrm{pH} = 0) - 0.06 \times \mathrm{pH} \quad (7)$$

Other small potential-determining cations (Li^+, Na^+) may alternatively be used in aprotic solvents to shift the band positions, with their potential-determining ability related to the ability of the cations to intercalate into the semiconductor lattice [175,181,209,210].

We have examined the pH dependence of electron injection rate from Ru535 and 470 to TiO_2 [143]. A comparison of electron injection rate from Ru470 to TiO_2 at pH 2, 4, 6, 8 is shown in Fig. 8. The injection dynamics are biphasic with a < 100 fs fast component and slower components. The amplitude of the fast component decreases and the rate of the slow components become slower with increasing pH. Similar pH dependence was observed for Ru535.

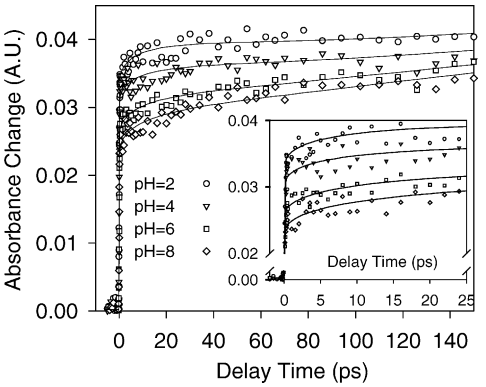

Fig. 8. Comparison of electron absorption dynamics of Ru470 sensitized TiO_2 films at different pHs. Open symbols are data and solid lines are fits. Inset: the same data plotted on a shorter time scale.

The dependence of injection dynamics on pH and cation concentration in solution have also been examined by other groups [105,181,182]. Durrant and co-workers [105] found that injection for Ru535/TiO_2 proceeds faster in solution with Li^+ cation present than when it was absent. Meyer and co-workers [181,182] examined the dependence of luminescence quantum yield on cation concentration and pH in Ru dye-sensitized TiO_2 film. At higher cation or proton concentration, they observed decreased sensitizer luminescence quantum yield, which suggests faster electron transfer rates. These dependences were attributed to the shifting of empty electron accepting states in semiconductor as a function of proton or cation concentration, consistent with our observation.

Change of pH or cation concentration may also affect the adsorbate energetics and its binding with the nanoparticle [163,211,212], both of which affect the injection rate. A better way of controlling electron accepting state density may be to change external bias [105,139]. Application of a more negative potential raises the Fermi level in the semiconductor, decreasing the availability of accepting states at a given energy, thus retarding the injection. Tachibana and co-workers [105] observed a retardation of injection rate from Ru535 to TiO_2 at more negative bias, consistent with the expected change in the number of accepting states. Iwai and co-workers [139] also observed a similar trend in interfacial charge separation rate in $Ru(bpy)_2(dcbpy)/SnO_2$.

It appears that same trend of change in injection dynamics is observed by lowering the dye excited state oxidation potential down towards the conduction band edge (comparing different dyes at the same pH), by raising the conduction band edge (comparing same dye at different pH or cation concentration), or by raising the Fermi level in the semiconductor. This provides support of the important role of density of accepting states in determining interfacial electron transfer rate.

7. Summary and future work

We have demonstrated that the electron transfer dynamics between semiconductor nanoparticles and molecular adsorbates can be studied using femtosecond mid-IR spectroscopy. With this technique, both the adsorbate vibrational spectral change and the mid-IR absorption of injected electrons can be simultaneously monitored. The direct observation of injected electrons allows for unambiguous assignment of electron transfer processes. Using this technique and complementary techniques in the visible region, we have started to systematically examine dependence of electron injection rates on the components of molecular (donor)–bridge–anchor–nanoparticle systems. These dependencies are understood by comparing with Marcus' theory of interfacial electron transfer.

Electron injection from Ru535 and derivatives to TiO_2 were found to be biphasic, with the <100 fs fast component and slower components. This behavior was attributed to the competition of ultrafast electron injection from unthermalized excited state and intramolecular relaxation within the excited state manifold. To account for this behavior, a two-state injection model was proposed. Evidence for injection from unthermalized state was obtained by choosing sensitizers that were not capable of injecting from the relaxed excited state. ReC0 on dry TiO_2 film served as an example. Evidence of the competition of the injection and relaxation pathways was demonstrated in ReC1/TiO_2 by slowing down the injection rate so that it is no longer competitive with intramolecular relaxation, which leads to injection kinetics dominated by slow injection components from the relaxed state. Excitation wavelength dependent injection kinetics were observed to provide further evidence for injection from unrelaxed excited state. In addition to TiO_2, biphasic injection kinetics were also observed from Ru535 to SnO_2 and ZnO, although these kinetics showed much smaller fast components and dominating slower components. We suggest that the biphasic injection is a consequence of the large energetic separation and fast relaxation between the Franck–Condon state and the thermalized excited state in these transition metal complexes.

The dependence of ET rate on electronic coupling was studied in SnO_2 films sensitized by a series of modified $Re(dcbpy)(CO)_3Cl$ complexes: ReCn (n = 0–5). These complexes have n CH_2 spacer groups between the bipyridine and carboxylate groups, corresponding to decreasing electronic coupling to TiO_2. We found that for n = 3–5 the rate decreased exponentially with the number of CH_2 spacers with decay constant β_n = 1, consistent with earlier studies for longer methylene spacers. However, for n = 1 and 2, ET rates are similar, deviating from exponential dependence. The origin of the deviation is still under investigation. Ongoing studies are examining these sensitizers on other semiconductors and under different solvent environment. Furthermore, coupling dependence study will be carried out with other short spacer groups. Other approaches to change coupling, such as modifying the anchoring group, are also explored.

One significant difference between ET to semiconductor (or metal) and intramolecular ET is the existence of a continuum of electron accepting states. As a result, ET rate depends on the density of accepting states, which depends on the relative potential of adsorbate versus conduction band edge in a semiconductor. This dependence was examined by varying both the adsorbate potential and the conduction band edge position. Electron injection dynamics were compared in TiO_2 and SnO_2 films sensitized by a series of $Ru(dcbpy)_2X_2$ (X_2 = $2SCN^-$, $2CN^-$, and dcbpy) dyes, which have different excited state redox potentials. The ET rate is slower for adsorbates with lower redox potential, qualitatively consistent with the corresponding decrease of electron accepting state density. The pH dependence of electron injection from Ru535 and 470 to TiO_2 was also examined. At higher pH, injection rate decreases, consistent with a higher conduction band edge position and therefore lower electron accepting state density.

Our studies have revealed some qualitative trends for interfacial ET dynamics. Systematic studies designed to quantitatively test interfacial ET theory are ongoing. A quantitative comparison of experimentally measured ET rates with theoretical predictions will require much better characterization of density of states of the nanomaterials and their electronic coupling with the adsorbate. Sophisticated surface science techniques may be needed to characterize these nanoparticles. Advanced computational studies of ET between nanoparticle and adsorbate will most likely be necessary [46–48,213–217]. The dependence of ET rate on other parameters will also be investigated. The dependence on solvent reorganization energy can also be examined by performing similar studies on films in contact with different solvents. Another potentially fruitful direction is to combine this technique with electrochemical studies, which allows control of the energetics of the semiconductor. A very challenging and yet very important direction is the dependence of injection rate on the nature of semiconductor. Although not completely understood, preliminary results indicate significant difference in injection rate from Ru535 to TiO_2, SnO_2 and ZnO, which likely caused by both the changes of state density and electron coupling strength. The effect of quantum confinement [22,32,218] on electron transfer dynamics in quantum dots should also be examined.

Acknowledgment

We dedicate this paper to Dr. Michael Gratzel on his 60th birthday. This work is supported by the Division of Chemical Sciences of the US Department of Energy and in part by the Petroleum Research Fund, administered by the ACS and the Emory University Research Committee. T.L. is a recipient of the National Science Foundation CAREER award and Sloan fellowship. We would like to thank R.J. Ellingson, S. Ferrere, and A.J. Nozik from NREL for their contribution in the Ru535/TiO_2 study and D. Chen and D.L. Mohler for their contribution to the electronic coupling dependence study of ReCn/SnO2. T.L. would like to thank Drs. M. Gratzel, G.V. Hartland, J.T. Hupp, J.K. McCusker, G.J. Meyer, R.J.D. Miller, M.D. Newton, A. Nozik, D. Waldeck, F. Willig, and J. Zhang for stimulating discussions.

References

[1] R.J.D. Miller, G.L. McLendon, A.J. Nozik, W. Schmickler, F. Willig, Surface Electron Transfer Processes, VCH Publishers Inc., 1995.
[2] A. Hagfeldt, M. Gratzel, Chem. Rev. 95 (1995) 49.
[3] P.V. Kamat, Chem. Rev. 93 (1993) 267.
[4] P.V. Kamat, Prog. React. Kinet. 19 (1994) 277.
[5] P.V. Kamat, D. Meisel, Semiconductor Nanoclusters: Physical, Chemicaland Catalytic Aspects, Elsevier, Amsterdam, 1997.
[6] J.B. Asbury, E. Hao, Y. Wang, H.N. Ghosh, T. Lian, J. Phys. Chem. B 105 (2001) 4545.
[7] B. O'Regan, M. Gratzel, Nature 353 (1991) 737.
[8] U. Bach, D. Lupo, P. Comte, J.E. Moser, F. Weissortel, J. Salbeck, H. Spreitzer, M. Gratzel, Nature 395 (1998) 583.
[9] W.U. Huynh, J.J. Dittmer, A.P. Alivisatos, Science 295 (2002) 2425.
[10] N. Serpone, E. Pelizzetti (Eds.), Photocatalysis, Fundamentals and Applications, John Wiley & Sons, 1989.
[11] V.L. Colvin, M.C. Schlamp, A.P. Alivisatos, Nature 370 (1994) 354.
[12] A. Aviram, M.A. Ratner, Chem. Phys. Lett. 29 (1974) 277.
[13] A. Nitzan, M. Ratner, Science 300 (2003) 1384.
[14] D. Segal, A. Nitzan, W.B. Davis, M.R. Wasielewski, M.A. Ratner, J. Phys. Chem. B 104 (2000) 3817.
[15] A. Nitzan, Annu. Rev. Phys. Chem. 52 (2001) 681.
[16] A. Nitzan, J. Phys. Chem. A 105 (2001) 2677.
[17] N.C. Greenham, X.G. Peng, A.P. Alivisatos, Synth. Met. 84 (1997) 545.
[18] W.U. Huynh, X.G. Peng, A.P. Alivisatos, Adv. Mater. 11 (1999) 923.
[19] A.C. Arango, S.A. Carter, P.J. Brock, Appl. Phys. Lett.. 74 (1999) 1698.
[20] S.E. Shaheen, C.J. Brabec, N.S. Sariciftci, F. Padinger, T. Fromherz, J.C. Hummelen, Appl. Phys. Lett. 78 (2001) 841.
[21] M.K. Nazeeruddin, A. Kay, I. Rodicio, R. Humphrybaker, E. Muller, P. Liska, N. Vlachopoulos, M. Gratzel, J. Am. Chem. Soc. 115 (1993) 6382.
[22] M.L. Steigerwald, L.E. Brus, Acc. Chem. Res. 23 (1990) 183.
[23] V.I. Klimov, D.W. McBranch, C.A. Leatherdale, M.G. Bawendi, Phys. Rev. B: Condens. Matter 60 (1999) 13740.
[24] D.J. Norris, A.L. Efros, M. Rosen, M.G. Bawendi, Phys. Rev. B: Condens. Matter 53 (1996) 16347.
[25] A.P. Alivisatos, Science 271 (1996) 933.
[26] D. Yu, C. Wang, P. Guyot-Sionnest, Science 300 (2003) 1277.
[27] B.L. Wehrenberg, P. Guyot-Sionnest, J. Am. Chem. Soc. 125 (2003) 7806.
[28] C. Wang, M. Shim, P. Guyot-Sionnest, Science 291 (2001) 2390.
[29] R.A. Marcus, N. Sutin, Biochem. Biophys. Acta 811 (1985) 265.
[30] M.D. Newton, Chem. Rev. 91 (1991) 767.
[31] P.F. Barbara, T.J. Meyer, M.A. Ratner, J. Phys. Chem. 100 (1996) 13148.
[32] A.P. Alivisatos, J. Phys. Chem. 100 (1996) 13226.
[33] S. Empedocles, M. Bawendi, Acc. Chem. Res. 32 (1999) 389.
[34] M. Nirmal, B.O. Dabbousi, M.G. Bawendi, J.J. Macklin, J.K. Trautman, T.D. Harris, L.E. Brus, Nature 383 (1996) 802.
[35] J.Z. Zhang, Acc. Chem. Res. 30 (1997) 423.
[36] J. Zhang, J. Phys. Chem. B 104 (2000) 7239.
[37] V.I. Klimov, J. Phys. Chem. B 104 (2000) 6112.
[38] J.H. Hodak, I. Martini, G.V. Hartland, J. Phys. Chem. B 102 (1998) 6958.
[39] S. Link, M.A. El-Sayed, Int. Rev. Phys. Chem. 19 (2000) 409.
[40] S. Link, M.A. El-Sayed, J. Phys. Chem. B 103 (1999) 8410.
[41] A.J. Nozik, Annu. Rev. Phys. Chem. 52 (2001) 193.
[42] J.M. Lanzafame, S. Palese, D. Wang, R.J.D. Miller, A.A. Muenter, J. Phys. Chem. 98 (1994) 11020.
[43] R.A. Marcus, J. Chem. Phys. 43 (1965) 679.
[44] H. Gerischer, Semiconductor electrochemistry, in: H. Eyring, D. Henderson, W. Jost (Eds.), In: Physical Chemistry: An Advance Treatise, vol. 9A, Academic Press, New York, 1970, p. 463.
[45] V.G. Levich, R.R. Dogonadze, Dokl. Akad. Nauk SSSR 124 (1959) 123.
[46] Y.Q. Gao, Y. Georgievskii, R.A. Marcus, J. Chem. Phys. 112 (2000) 3358.
[47] Y.Q. Gao, R.A. Marcus, J. Chem. Phys. 113 (2000) 6351.
[48] S. Gosavi, R.A. Marcus, J. Phys. Chem. B 104 (2000) 2067.
[49] J. Nelson, S.A. Haque, D.R. Klug, J.R. Durrant, Phys. Rev. B: Condens. Matter Mater. Phys. 63 (2001) 205321.

[50] J. Nelson, Phys. Rev. B: Condens. Matter Mater. Phys. 59 (1999) 15374.
[51] G. Rothenberger, D. Fitzmaurice, M. Gratzel, J. Phys. Chem. 96 (1992) 5983.
[52] G. Boschloo, D. Fitzmaurice, J. Phys. Chem. B 103 (1999) 2228.
[53] N.W. Duffy, L.M. Peter, R.M.G. Rajapakse, K.G.U. Wijayantha, Electron. Commun. 2 (2000) 658.
[54] R.L. Willis, C. Olson, B. O'Regan, T. Lutz, J. Nelson, J.R. Durrant, J. Phys. Chem. B 106 (2002) 7605.
[55] J.B. Asbury, Y. Wang, T. Lian, J. Phys. Chem. B 103 (1999) 6643.
[56] J.B. Asbury, E. Hao, Y. Wang, T. Lian, J. Phys. Chem. B 104 (2000) 11957.
[57] S. Ramakrishna, F. Willig, V. May, Phys. Rev. B: Condens. Matter Mater. Phys. 62 (2000) 16330.
[58] S. Ramakrishna, F. Willig, J. Phys. Chem. B 104 (2000) 68.
[59] S. Ramakrishna, F. Willig, V. May, J. Chem. Phys. 115 (2001) 2743.
[60] S. Ramakrishna, F. Willig, V. May, Chem. Phys. Lett. 351 (2002) 242.
[61] R. Memming, Top. Curr. Chem. 169 (1994) 105.
[62] N.S. Lewis, Annu. Rev. Phys. Chem. 42 (1991) 543.
[63] A.J. Nozik, R. Memming, J. Phys. Chem. 100 (1996) 13061.
[64] X.D. Cui, A. Primak, X. Zarate, J. Tomfohr, O.F. Sankey, A.L. Moore, T.A. Moore, D. Gust, G. Harris, S.M. Lindsay, Science 294 (2001) 571.
[65] J.F. Smalley, H.O. Finklea, C.E.D. Chidsey, M.R. Linford, S.E. Creager, J.P. Ferraris, K. Chalfant, T. Zawodzinsk, S.W. Feldberg, M.D. Newton, J. Am. Chem. Soc. 125 (2003) 2004.
[66] J.F. Smalley, S.W. Feldberg, C.E.D. Chidsey, M.R. Linford, M.D. Newton, Y.P. Liu, J. Phys. Chem. 99 (1995) 13141.
[67] C.E.D. Chidsey, Science 251 (1991) 919.
[68] S.B. Sachs, S.P. Dudek, R.P. Hsung, L.R. Sita, J.F. Smalley, M.D. Newton, S.W. Feldberg, C.E.D. Chidsey, J. Am. Chem. Soc. 119 (1997) 10563.
[69] Y. Gu, D.H. Waldeck, J. Phys. Chem. B 102 (1998) 9015.
[70] Y. Gu, D.H. Waldeck, J. Phys. Chem. 100 (1996) 9573.
[71] L.-H. Guo, J.S. Facci, G. McLendon, J. Phys. Chem. 99 (1995) 8458.
[72] C. Miller, M. Gratzel, J. Phys. Chem. 95 (1991) 5225.
[73] A.M. Becka, C.J. Miller, J. Phys. Chem. 96 (1992) 2657.
[74] H.O. Finklea, D.D. Hanshew, J. Am. Chem. Soc. 114 (1992) 3173.
[75] S. Creager, C.J. Yu, C. Bamdad, S. O'Connor, T. MacLean, E. Lam, Y. Chong, G.T. Olsen, J. Luo, M. Gozin, J.F. Kayyem, J. Am. Chem. Soc. 121 (1999) 1059.
[76] K.S. Weber, S.E. Creager, J. Electroanal. Chem. 458 (1998) 17.
[77] N.S. Lewis, J. Phys. Chem. B 102 (1998) 4843.
[78] A.M. Fajardo, N.S. Lewis, Science 274 (1996) 969.
[79] A.J. Bard, L.R. Faulkner, Electrochemical Methods: Fundamentals and Applications, second ed., John Wiley & Sons Inc., 2001.
[80] H.-L. Dai, W. Ho (Eds.), Laser Spectroscopy and Photochemistry on Metal Surface, Parts I & II, vol. 5, World Scientific Publishing Co., Singapore, 1995.
[81] W. Ho, Surf. Sci. 300 (1994) 996.
[82] J.P. Culver, M. Li, Z.J. Sun, R.M. Hochstrasser, A.G. Yodh, Chem. Phys. 205 (1996) 159.
[83] J.P. Culver, M. Li, R.M. Hochstrasser, A.G. Yodh, Surf. Sci. 368 (1996) 9.
[84] C.M. Wong, J.D. McNeill, K.J. Gaffney, N.H. Ge, A.D. Miller, S.H. Liu, C.B. Harris, J. Phys. Chem. B 103 (1999) 282.
[85] C.B. Harris, N.H. Ge, R.L. Lingle, J.D. McNeill, C.M. Wong, Annu. Rev. Phys. Chem. 48 (1997) 711.
[86] A. Peremans, A. Tadjeddine, W.Q. Zheng, A. LeRille, P. Guyot-Sionnest, P.A. Thiry, Surf. Sci. 368 (1996) 384.
[87] X.Y. Zhu, Annu. Rev. Phys. Chem. 53 (2002) 221.
[88] K.B. Eisenthal, Chem. Rev. 96 (1996) 1343.
[89] Y.R. Shen, Solid State Commun. 102 (1997) 221.
[90] G.L. Richmond, Anal. Chem. 69 (1997) 536.
[91] J.M. Rehm, G.L. McLendon, Y. Nagasawa, K. Yoshihara, J. Moser, M. Gratzel, J. Phys. Chem. 100 (1996) 9577.
[92] F. Willig, R. Eichberger, N.S. Sundaresan, B.A. Parkinson, J. Am. Chem. Soc. 112 (1990) 2702.
[93] T.A. Heimer, G.J. Meyer, J. Lumin. 70 (1996) 468.
[94] Y. Rosenwaks, B.R. Thacker, R.K. Ahrenkiel, A.J. Nozik, J. Phys. Chem. 96 (1992) 10096.
[95] Y. Rosenwaks, B.R. Thacker, A.J. Nozik, R.J. Ellingson, K.C. Burr, C.L. Tang, J. Phys. Chem. 98 (1994) 2739.
[96] G.N. Ryba, C.N. Kenyon, N.S. Lewis, J. Phys. Chem. 97 (1993) 13814.
[97] S.J. Rosenthal, X.L. Xie, M. Du, G.R. Fleming, J. Chem. Phys. 95 (1991) 4715.
[98] H.P. Lu, X.S. Xie, J. Phys. Chem. B 101 (1997) 2753.
[99] L. Zhang, R. Liu, M.W. Holman, K.T. Nguyen, D.M. Adams, J. Am. Chem. Soc. 124 (2002) 10640.
[100] G.R. Fleming, Chemical Applications of Ultrafast Spectroscopy, Oxford University Press, New York, 1986.
[101] E. Palomares, J.N. Clifford, S.A. Haque, T. Lutz, J.R. Durrant, J. Am. Chem. Soc. 125 (2003) 475.
[102] S.A. Haque, T. Park, A.B. Holmes, J.R. Durrant, Chem. Phys. Chem. 4 (2003) 89.
[103] Y. Tachibana, M.K. Nazeeruddin, M. Gratzel, D.R. Klug, J.R. Durrant, Chem. Phys. 285 (2002) 127.
[104] J.R. Durrant, J. Photochem. Photobiol. A: Chem. 148 (2002) 5.
[105] Y. Tachibana, S.A. Haque, I.P. Mercer, J.E. Moser, D.R. Klug, J.R. Durrant, J. Phys. Chem. B 105 (2001) 7424.
[106] Y. Tachibana, S.A. Haque, I.P. Mercer, J.R. Durrant, D.R. Klug, J. Phys. Chem. B 104 (2000) 1198.
[107] S.A. Haque, Y. Tachibana, R.L. Willis, J.E. Moser, M. Graetzel, D.R. Klug, J.R. Durrant, J. Phys. Chem. B 104 (2000) 538.
[108] J.R. Durrant, Y. Tachibana, I. Mercer, J.E. Moser, M. Gratzel, D.R. Klug, Z. Phys. Chem. 212 (1999) 93.
[109] U. Bach, Y. Tachibana, J.-E. Moser, S.A. Haque, J.R. Durrant, M. Graetzel, D.R. Klug, J. Am. Chem. Soc. 121 (1999) 7445.
[110] S.A. Haque, Y. Tachibana, D.R. Klug, J.R. Durrant, J. Phys. Chem. B 102 (1998) 1745.
[111] Y. Tachibana, J.E. Moser, M. Graetzel, D.R. Klug, J.R. Durrant, J. Phys. Chem. 100 (1996) 20056.
[112] C. Zimmermann, F. Willig, S. Ramakrishna, B. Burfeindt, B. Pettinger, R. Eichberger, W. Storck, J. Phys. Chem. B 105 (2001) 9245.
[113] B. Burfeindt, C. Zimmermann, S. Ramakrishna, T. Hannappel, B. Meissner, W. Storck, F. Willig, Zeitschrift fuer Physikalische Chemie (Muenchen) 212 (1999) 67.
[114] B. Burfeindt, S. Ramakrishna, C. Zimmermann, B. Meissner, T. Hannappel, W. Storck, F. Willig, Measurement and Theoretical Modelling of Ultrafast Heterogeneous Spacer-Controlled Electron Transfer, Ultrafast Phenomena XI, 1998.
[115] F. Willig, B. Burfeindt, K. Schwarzburg, T. Hannappel, W. Storck, Proc. Indian Acad. Sci. Chem. Sci. 109 (1997) 415.
[116] T. Hannappel, B. Burfeindt, W. Storck, F. Willig, J. Phys. Chem. B 101 (1997) 6799.
[117] B. Burfeindt, T. Hannapel, W. Storck, F. Willig, J. Phys. Chem. 100 (1996) 16463.
[118] G. Benko, B. Skarman, R. Wallenberg, A. Hagfeldt, V. Sundstrom, A.P. Yartsev, J. Phys. Chem. B 107 (2003) 1370.
[119] G. Benko, P. Myllyperkio, J. Pan, A.P. Yartsev, V. Sundstrom, J. Am. Chem. Soc 125 (2003) 1118.
[120] J. Kallioinen, G. Benko, V. Sundstrom, J.E.I. Korppi-Tommola, A.P. Yartsev, J. Phys. Chem. B 106 (2002) 4396.
[121] G. Benko, J. Kallioinen, J.E.I. Korppi-Tommola, A.P. Yartsev, V. Sundstrom, J. Am. Chem. Soc. 124 (2002) 489.
[122] I. Martini, J.H. Hodak, G.V. Hartland, J. Phys. Chem. B 103 (1999) 9104.
[123] I. Martini, J.H. Hodak, G.V. Hartland, J. Phys. Chem. B 102 (1998) 607.

[124] I. Martini, J.H. Hodak, G.V. Hartland, J. Phys. Chem. B 102 (1998) 9508.
[125] I. Martini, J. Hodak, G.V. Hartland, P.V. Kamat, J. Chem. Phys. 107 (1997) 8064.
[126] F. Parsapour, D.F. Kelley, S. Craft, J.P. Wilcoxon, J. Chem. Phys. 104 (1996) 4978.
[127] C.I. Butoi, B.T. Langdon, D.F. Kelley, J. Phys. Chem. B 102 (1998) 9635.
[128] V. Chikan, M.R. Waterland, J.M. Huang, D.F. Kelley, J. Chem. Phys. 113 (2000) 5448.
[129] C.M. Olsen, M.R. Waterland, D.F. Kelley, J. Phys. Chem. B 106 (2002) 6211.
[130] N.J. Cherepy, G.P. Smestad, M. Gratzel, J.Z. Zhang, J. Phys. Chem. 101 (1997) 9342.
[131] D. Kuciauskas, M.S. Freund, H.B. Gray, J.R. Winkler, N.S. Lewis, J. Phys. Chem. B 105 (2001) 392.
[132] D. Kuciauskas, J.E. Monat, R. Villahermosa, H.B. Gray, N.S. Lewis, J.K. McCusker, J. Phys. Chem. B 106 (2002) 9347.
[133] K. Kilsa, E.I. Mayo, D. Kuciauskas, R. Villahermosa, N.S. Lewis, J.R. Winkler, H.B. Gray, J. Phys. Chem. A 107 (2003) 3379.
[134] R. Huber, S. Sporlein, J.E. Moser, M. Gratzel, J. Wachtveitl, J. Phys. Chem. B 104 (2000) 8995.
[135] R. Huber, J.E. Moser, M. Gratzel, J. Wachtveitl, J. Phys. Chem. B 106 (2002) 6494.
[136] R. Katoh, A. Furube, K. Hara, S. Murata, H. Sugihara, H. Arakawa, M. Tachiya, J. Phys. Chem. B 106 (2002) 12957.
[137] A. Furube, R. Katoh, K. Hara, S. Murata, H. Arakawa, M. Tachiya, J. Phys. Chem. B 107 (2003) 4162.
[138] H. Horiuchi, R. Katoh, K. Hara, M. Yanagida, S. Murata, H. Arakawa, M. Tachiya, J. Phys. Chem. B 107 (2003) 2570.
[139] S. Iwai, K. Hara, S. Murata, R. Katoh, H. Sugihara, H. Arakawa, J. Chem. Phys. 113 (2000) 3366.
[140] P. Piotrowiak, E. Galoppini, Q. Wei, G.J. Meyer, P. Woewior, J. Am. Chem. Soc. 125 (2003) 5278.
[141] T.A. Heimer, E.J. Heilweil, C.A. Bignozzi, G.J. Meyer, J. Phys. Chem. A 104 (2000) 4256.
[142] T. Heimer, E.J. Heilweil, J. Phys. Chem. B 101 (1997) 10990.
[143] J.B. Asbury, N.A. Anderson, E. Hao, T. Lian, J. Phys. Chem. B 107 (2003) 7376.
[144] N.A. Anderson, X. Ai, D. Chen, D.L. Mohler, T. Lian, J. Phys. Chem. B, in press.
[145] E. Hao, N.A. Anderson, J.B. Asbury, T. Lian, J. Phys. Chem. B 106 (2002) 10191.
[146] J.B. Asbury, Y.Q. Wang, E.C. Hao, H.N. Ghosh, T. Lian, Res. Chem. Interm. 27 (2001) 315.
[147] N.A. Anderson, E. Hao, X. Ai, G. Hastings, T. Lian, Chem. Phys. Lett. 347 (2001) 304.
[148] Y.-X. Weng, Y.-Q. Wang, J.B. Asbury, H.N. Ghosh, T. Lian, J. Phys. Chem. B 104 (2000) 93.
[149] Y. Wang, J.B. Asbury, T. Lian, J. Phys. Chem. A 104 (2000) 4291.
[150] H.N. Ghosh, J.B. Asbury, T. Lian, PINSA-A: Proc. Indian Natl. Sci. Acad., Part A 66 (2000) 177.
[151] R.J. Ellingson, J.B. Asbury, S. Ferrere, H.N. Ghosh, J.R. Sprague, T. Lian, A.J. Nozik, Z. Phys. Chem. (Muenchen) 212 (1999) 77.
[152] J.B. Asbury, R.J. Ellingson, H.N. Ghosh, S. Ferrere, A.J. Nozik, T. Lian, J. Phys. Chem. B 103 (1999) 3110.
[153] H.N. Ghosh, J.B. Asbury, T. Lian, J. Phys. Chem. B 102 (1998) 6482.
[154] H.N. Ghosh, J.B. Asbury, Y. Weng, T. Lian, J. Phys. Chem. B 102 (1998) 10208.
[155] R.J. Ellingson, J.B. Asbury, S. Ferrere, H.N. Ghosh, J.R. Sprague, T. Lian, A.J. Nozik, J. Phys. Chem. B 102 (1998) 6455.
[156] N.A. Anderson, X. Ai, T. Lian, J. Phys. Chem. B, in press.
[157] J.I. Pankove, Optical Processes in Semiconductors, Dover, New York, 1975.
[158] P. Guyot-Sionnest, M.A. Hines, Appl. Phys. Lett. 72 (1998) 686.
[159] P. Guyot-Sionnest, M. Shim, C. Matranga, M. Hines, Phys. Rev. B: Condens. Matter 60 (1999) 2181.
[160] M. Shim, S.V. Shilov, M.S. Braiman, P. Guyot-Sionnest, J. Phys. Chem. B 104 (2000) 1494.
[161] V.I. Klimov, C.J. Schwarz, D.W. McBranch, C.A. Leatherdale, M.G. Bawendi, Phys. Rev. B: Condens. Matter 60 (1999) 2177.
[162] J.B. Asbury, E.C. Hao, T. Lian, in preparation.
[163] A. Zaban, S. Ferrere, J. Sprague, B.A. Gregg, J. Phys. Chem. B 101 (1997) 55.
[164] D.L. Mohler, D. Chen, V.B. Reddy, Synthesis (2002) 745.
[165] J.H. Rodriguez, J.K. McCusker, J. Chem. Phys. 116 (2002) 6253.
[166] A.T. Yeh, C.V. Shank, J.K. McCusker, Springer Ser. Chem. Phys. 66 (2001) 494.
[167] N.H. Damrauer, G. Cerullo, A. Yeh, T.R. Boussie, C.V. Shank, J.K. McCusker, Science 275 (1997) 54.
[168] N.H. Damrauer, J.K. McCusker, J. Phys. Chem. A 103 (1999) 8440.
[169] A.C. Bhasikuttan, M. Suzuki, S. Nakashima, T. Okada, J. Am. Chem. Soc. 124 (2002) 8398.
[170] G. Sauve, M.E. Cass, G. Coia, S.J. Doig, I. Lauermann, K.E. Pomykal, N.S. Lewis, J. Phys. Chem. B 104 (2000) 6821.
[171] L.A. Worl, R. Duesing, P. Chen, L.D. Ciana, T.J. Meyer, J. Chem. Soc., Dalton Trans. (1991) 849.
[172] P.I. Sorantin, K. Scharz, Inorg. Chem. 31 (1992) 567.
[173] V. Henrich, P. Cox, The Surface Science of Metal Oxides, Cambridge University Press, Cambridge, 1996.
[174] R. Hoffmann, Solids and Surfaces: A Chemist's View of Bonding in Extended Structures, Wiley/VCH Inc., 1988.
[175] G. Redmond, A. O'Keeffe, C. Burgess, C. MacHale, D. Fitzmaurice, J. Phys. Chem. 97 (1993) 11081.
[176] B. Enright, D. Fitzmaurice, J. Phys. Chem. 100 (1996) 1027.
[177] K. Kalyanasundaram, Photochemistry of Polypyridine and Porphyrin Complexes, Academic Press, London, 1992.
[178] J.E. Moser, M. Gratzel, Chimia 52 (1998) 160.
[179] J.E. Moser, M. Wolf, F. Lenzmann, M. Gratzel, Z. Phys. Chem. (Muenchen) 212 (1999) 85.
[180] C.A. Kelly, F. Farzad, D.W. Thompson, G. Meyer, J. Langmuir 15 (1999) 731.
[181] C.A. Kelly, F. Farzad, D.W. Thompson, J.M. Stipkala, G.J. Meyer, Langmuir 15 (1999) 7047.
[182] P. Qu, G.J. Meyer, Langmuir 17 (2001) 6720.
[183] F. Lenzmann, J. Krueger, S. Burnside, K. Brooks, M. Graetzel, D. Gal, S. Ruehle, D. Cahen, J. Phys. Chem. B 105 (2001) 6347.
[184] S. Ferrere, B.A. Gregg, J. Am. Chem. Soc. 120 (1998) 843.
[185] C.X. Liang, M.D. Newton, J. Phys. Chem. 97 (1993) 3199.
[186] C.X. Liang, M.D. Newton, J. Phys. Chem. 96 (1992) 2855.
[187] L.A. Curtiss, J.R. Miller, J. Phys. Chem. A 102 (1998) 160.
[188] L.A. Curtiss, C.A. Naleway, J.R. Miller, J. Phys. Chem. 97 (1993) 4050.
[189] C.-P. Hsu, J. Electroanal. Chem. 438 (1997) 27.
[190] C.-P. Hsu, R.A. Marcus, J. Chem. Phys. 106 (1997) 584.
[191] K.D. Jordan, M.N. Paddon-Row, Chem. Rev. 92 (1992) 395.
[192] C.K. Ryu, R. Wang, R.H. Schmehl, S. Ferrere, M. Ludwikow, J.W. Merkert, C.E.L. Headford, C.M. Elliott, J. Am. Chem. Soc. 114 (1992) 430.
[193] K.S. Schanze, K.A. Walters, in: V. Ramamurthy, K.S. Schanze (Eds.), Organic and Inorganic Photochemistry, vol. 2, Marcel-Dekker, New York, 1998, p. 75.
[194] S.L. Larson, C.M. Elliott, D.F. Kelley, J. Phys. Chem. 99 (1995) 6530.
[195] E.H. Yonemoto, Y.I. Kim, R.H. Schmehl, J.O. Wallin, B.A. Shoulders, B.R. Richardson, J.F. Haw, T.E. Mallouk, J. Am. Chem. Soc. 116 (1994) 10557.
[196] E.H. Yonemoto, G.B. Saupe, R.H. Schmehl, S.M. Hubig, R.L. Riley, B.L. Iverson, T.E. Mallouk, J. Am. Chem. Soc. 116 (1994) 4786.

[197] D.E. Khoshtariya, T.D. Dolidze, L.D. Zusman, D.H. Waldeck, J. Phys. Chem. A 105 (2001) 1818.
[198] H.D. Sikes, J.F. Smalley, S.P. Dudek, A.R. Cook, M.D. Newton, C.E.D. Chidsey, S.W. Feldberg, Science 291 (2001) 1519.
[199] P.G. Hoertz, R.A. Carlisle, G.J. Meyer, D. Wang, P. Piotrowiak, E. Galoppini, Nano Lett. 3 (2003) 325.
[200] E. Galoppini, W. Guo, W. Zhang, P.G. Hoertz, P. Qu, G.J. Meyer, J. Am. Chem. Soc. 124 (2002) 7801.
[201] E. Galoppini, W. Guo, P. Qu, G.J. Meyer, J. Am. Chem. Soc. 123 (2001) 4342.
[202] I. Gillaizeau-Gauthier, F. Odobel, M. Alebbi, R. Argazzi, E. Costa, C.A. Bignozzi, P. Qu, G. Meyer, J. Inorg. Chem. 40 (2001) 6073.
[203] T.A. Heimer, S.T. D'Arcangelis, F. Farzad, J.M. Stipkala, G. Meyer, J. Inorg. Chem. 35 (1996) 5319.
[204] F. Odobel, E. Blart, M. Lagree, M. Villieras, H. Boujtita, N. El Murr, S. Caramori, C. Alberto Bignozzi, J. Mater. Chem. 13 (2003) 502.
[205] C. She, J. Hupp, T. Lian, unpublished result.
[206] J.M. Bolts, M.S. Wrighton, J. Phys. Chem. 80 (1976) 2641.
[207] L.A. Lyon, J.T. Hupp, J. Phys. Chem. B 103 (1999) 4623.
[208] B. Enright, G. Redmond, D. Fitzmaurice, J. Phys. Chem. 98 (1994) 6195.
[209] G. Redmond, D. Fitzmaurice, J. Phys. Chem. 97 (1993) 1426.
[210] G. Redmond, D. Fitzmaurice, M. Graetzel, J. Phys. Chem. 97 (1993) 6951.
[211] M.K. Nazeeruddin, S.M. Zakeerudin, R. Humphry-Baker, M. Jirousek, P. Liska, N. Vlachopoulos, V. Shklover, C.-H. Fischer, M. Gratzel, Inorg. Chem. 38 (1999) 6298.
[212] A. Zaban, S. Ferrere, B.A. Gregg, J. Phys. Chem. B 102 (1998) 452.
[213] B.B. Smith, J.W. Halley, A. Nozik, J. Chem. Phys. 205 (1996) 245.
[214] B.B. Smith, A. Nozik, J. Chem. Phys. 205 (1996) 47.
[215] Y.G. Boroda, G.A. Voth, J. Chem. Phys. 104 (1996) 6168.
[216] A. Calhoun, G.A. Voth, J. Phys. Chem. 100 (1996) 10746.
[217] C.P. Ursenbach, G.A. Voth, J. Chem. Phys. 103 (1995) 7569.
[218] M.G. Bawendi, M.L. Steigerwald, L.E. Brus, Ann. Rev. Phys. Chem. 41 (1990) 477.